

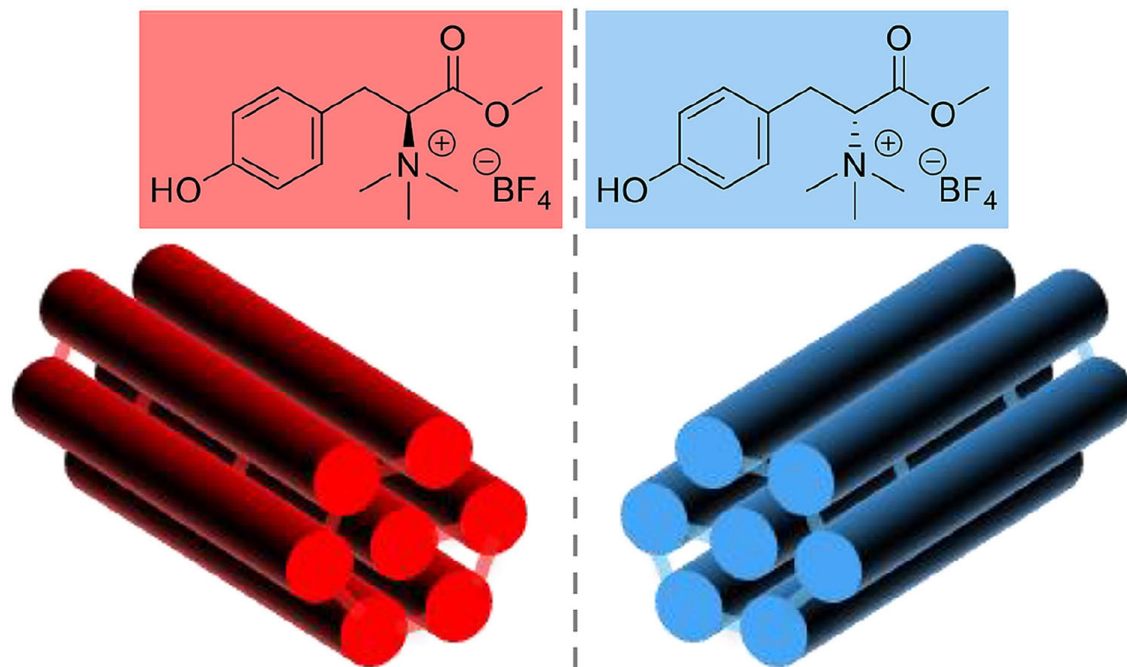


Published in final edited form as:

Perovic, M., Aloni, S. S., Mastai, Y., & Oschatz, M. (2020). Mesoporous carbon materials with enantioselective surface obtained by nanocasting for selective adsorption of chiral molecules from solution and the gas phase. *Carbon*, 170, 550-557. doi:10.1016/j.carbon.2020.08.010.

Mesoporous carbon materials with enantioselective surface obtained by nanocasting for selective adsorption of chiral molecules from solution and the gas phase

M. Perovic, S. S. Aloni, Y. Mastai, M. Oschatz



Graphical presentation of mesoporous chiral L-m-carbon (down left), and D-m-carbon (down right), together with their precursors – chiral ionic liquids, N,N,N-trimethyl-L-Tyrosine methyl ester tetrafluoroborate (top left), and N,N,N-trimethyl-D-Tyrosine methyl ester tetrafluoroborate (top right).

Mesoporous Carbon Materials With Enantioselective Surface Obtained by Nanocasting for Selective Adsorption of Chiral Molecules From Solution and the Gas Phase

Milena Perovic,^[a] Sapir Shekef Aloni,^[b] Yitzhak Mastai,^[b] Martin Oschatz^{*[a,c]}

[a] M. Perovic, Dr. M. Oschatz

Department of Colloid Chemistry, Max-Planck Institute of Colloids and Interfaces, Am Mühlenberg 1, 14476 Potsdam, Germany

E-mail: martin.oschatz@mpikg.mpg.de

[b] S. Shekef Aloni, Prof. Y. Mastai

Department of Chemistry and the Institute of Nanotechnology, Bar-Ilan University, Ramat-Gan 5290002, Israel

[c] Dr. M. Oschatz

University of Potsdam, Institute of Chemistry, Karl-Liebknecht-Str. 24-25, D-14476 Potsdam, Germany

Abstract

Separation of enantiomers is an everlasting challenge in chemistry, catalysis, and synthesis of pharmaceuticals. The design and fabrication of chiral adsorbent materials is a promising way to increase the surface area of chiral information, as well as to maximize the available surface for the adsorption of enantiomers. Porous materials such as silica or metal-organic-frameworks are established materials in this field, due to their well-defined surface structure and ease of functionalization with chiral groups. As another class of porous materials, carbons provide the advantages of high thermal and chemical stability, resistance against moisture, electrical conductivity, and widely tunable pore size. Although they are well established in many adsorption-related applications, carbons received far less attention in enantioselective adsorption processes because the controlled functionalization of their surface is rather difficult due to the electronically heterogeneous atoms in the network. A suitable approach to overcome this limitation is the synthesis of chiral carbons directly from chiral precursors. So far, chiral carbons

synthesized from chiral precursors used salt-templating as a way of introducing porosity, which resulted in mainly microporous materials or materials with broad pore size distribution. In the present study, the possibility of combining nanocasting as an alternative templating approach with chiral ionic liquids as a carbon precursor is demonstrated. Chiral recognition is measured in the gas phase, by adsorption of chiral gas, as well as in the solution, by using isothermal titration calorimetry.

Keywords: mesoporous carbon, chiral carbon, porous materials, enantiomers separation, chiral recognition, adsorption

1. Introduction

The separation of compounds with similar chemical composition but different chiral information is a crucial, but still challenging task in chemistry and catalysis.¹⁻³ A widely applied method to solve this problem is the enrichment of one chiral compound from a mixture of isomers by preferred physical adsorption (physisorption) on a surface containing chiral information itself. As one example, chiral high performance liquid chromatography has emerged as a powerful technique for separation and/or enantioselective chemical synthesis in recent years.⁴⁻⁵ To make these processes efficient, the chiral adsorbent material has to provide high surface area for functionalization with chiral information and for adsorption of the chiral compounds to be separated. Silica-based inorganic materials with chiral functional groups are widely established as stationary phases for such separations because their surface chemistry is rather well defined and controllable. Surface atoms in porous silica materials are all in a comparable chemical and electronic state, which makes it simple to perform a chiral surface modification through chemical reactions.⁶⁻⁷ Furthermore, their pore structure can be adjusted over a certain range.⁸⁻⁹ This makes it possible to optimize the stationary phase for the separation of chiral compounds of different sizes. Another obvious reason for the leading position of silica materials is that they are also well established as a stationary phase for other separation processes that can be achieved

with chromatographic methods. Another class of porous materials with controllable surface chemistry and pore structure which has been studied for chiral separation or catalysis purposes recently are metal-organic frameworks (MOFs).¹⁰⁻¹² MOFs can be functionalized with chiral groups by post-synthetic coupling/immobilization or by using linker molecules with chiral information directly during the synthesis of the framework.¹³⁻¹⁴ However, both MOFs and silica suffer from their limitations in terms of thermal stability, resistance against moisture, as well as low stability in the extreme pH regions. Moreover, MOFs are naturally limited to a relatively narrow range in terms of available pore sizes, and when approaching the smallest pore sizes, the pore size distribution of silica becomes rather broad.

Alternative candidates would be carbon nanomaterials, which have superior thermal and chemical stability. Another unique property of carbon that could be very useful in the context of enantioselective adsorption processes is its electric conductivity. It is widely known that the interaction of carbon with a given species to be adsorbed can be externally controlled by an applied electric potential.¹⁵⁻¹⁷ Furthermore, electric conductivity opens up the possibility of performing even asymmetric electrocatalysis.¹⁸⁻¹⁹ The chiral functionalization of carbon nanomaterials, such as carbon nanotubes (CNTs), fullerene or graphene, by simple attachment of chiral moieties to their edges was already reported in the literature.²⁰⁻²³ They have well-defined surface chemistry like silica or MOFs which makes it possible that a part of their surface can be uniformly decorated with chiral functions. For instance, a cap of a CNT or an edge of graphene is more reactive than the rest of the material, and this is exactly where the reaction for attachment of a chiral function would preferably take place. However, these carbon materials with defined atomic construction are not intrinsically porous and are thus less applicable for adsorption-based applications. Since this is of major importance for efficient chiral recognition and separation, porous carbon materials appear to be more suitable candidates.²⁴⁻²⁶ In comparison to silica, MOFs, and ordered carbon materials mentioned above, porous carbons have a less defined local atomic arrangement but they can possibly be prepared from renewable and sustainable

precursors and still provide electrical conductivity. As another major advantage over silica and MOFs, the pore architecture of carbons can be adjusted over a much broader range and carbons with a hierarchical pore architecture can be more easily synthesized.²⁷⁻²⁸ On the other hand, atoms (and in particular surface atoms) within ordinary porous carbon materials are usually chemically and electronically heterogeneous. Controlled functionalization of their surface is therefore challenging and can result in uneven distribution of various functional groups.²⁹⁻³¹ In that sense, the synthesis of chiral carbon materials directly from chiral precursors appears to be a promising approach for inserting chemically uniform chiral information into the final material. In a similar sense like the controlled condensation of precursor molecules leads to porous carbon materials with defined atomic construction,³²⁻³⁵ the carbonization of chiral precursors appears to be more suitable for the incorporation of uniform chiral groups than the post-synthetic coupling to an inhomogeneous surface.

A suitable and established method for achieving high surface area materials is templating, where a carbon precursor is combined with a non-carbonizable template that is removed after the carbonization.³⁶⁻³⁸ Recently, chiral porous carbon materials have been synthesized by using salt templating as a way of introducing porosity.³⁹⁻⁴⁰ This approach is suitable to synthesize chiral carbon materials with the high surface area but it remains limited to the fabrication of mainly microporous materials or materials with broad pore size distribution which may suffer from a large contribution of bottle-neck-shaped pores and non-discriminative surface. Furthermore, such materials would not be suitable for the separation of larger compounds which can simply not fit into the pores. From a kinetic point of view, larger pores with a defined size, geometry, and connectivity are often needed to enhance mass transport within the adsorbent and thus to minimize the time needed for the adsorption process to reach equilibrium.⁴¹ Therefore, our approach is to increase the pore size of chiral carbon materials by utilizing an alternative templating approach. We report the synthesis of mesoporous chiral carbon from a chiral ionic liquid (CIL) as a precursor, using the nanocasting technique with ordered mesoporous

silica as the template.^{36, 42} Chiral recognition of resulting material is demonstrated by the means of chiral gas adsorption, and isothermal titration calorimetry using enantiopure titrants. Molecular precursors for chiral carbon materials are combined with the nanocasting concept here for the first time as a proof of concept study for the synthesis of mesopore-containing chiral carbon compounds with a broad range of available pore sizes and notable chiral recognition.

2. Experimental Section

Synthesis of the ordered mesoporous chiral carbon

The hexagonal ordered silica template SBA-15 was synthesized by dissolving 33.4 g of the triblock copolymer Pluronic P123 (EO₂₀PO₇₀EO₂₀, Sigma Aldrich) in 606 g deionized water and 19.3 g concentrated aqueous hydrochloric acid solution overnight at 35 °C in a 1000 ml polypropylene bottle under intense stirring. Then, 71.8 g of tetraethyl orthosilicate (TEOS, 98 %, Sigma Aldrich) were added to the solution and the mixture was stirred at 35 °C for another 24 h. The white suspension was then transferred to a Teflon-lined autoclave and hydrothermally treated at 130 °C for 24 h followed by filtration and washing with ~1000 ml deionized water/ethanol (1:1 by volume). For the complete removal of the structure-directing agent, the SBA-15 was calcined at 550 °C for 5 h in a muffle furnace (60 °C h⁻¹ heating rate).⁴²

Ordered mesoporous chiral carbon was synthesized by impregnating 0.5 g of SBA-15 with a solution of 0.625 g chiral ionic liquid and 0.21 g trimesic acid in 3.5 mL water and 1.5 mL ethanol. Chiral ionic liquids, N,N,N-trimethyl-L-Tyrosine methyl ester tetrafluoroborate, and its D-enantiomer, were synthesized by a previously reported procedure.^{40, 43} The mixture was transferred to the Petri dish, dried at 100 °C for 6 h, and subsequently heated to 160 °C and kept for 6 h. Complete infiltration of template pores was achieved by repeating the procedure described above with a solution of 0.4 g chiral ionic liquid and 0.13 g trimesic acid in 3.5 mL water and 1.5 mL ethanol, again followed by heating to 100 °C and 160 °C. Carbonization was carried out under a flowing N₂ atmosphere in a horizontal tubular furnace. The material was heated to 500 °C (heating rate: 150 °C h⁻¹) and dwelled for 2 h. Silica removal was achieved by refluxing the carbonized composite material in sodium-hydroxide solution (100 mL, 5 mol L⁻¹) overnight. After filtration and washing with large amounts of ethanol, the chiral carbon was dried at 60 °C.

Characterization of carbon materials

Physisorption measurements

Prior to all of the physisorption measurements, the samples were outgassed under vacuum at 150 °C for 20 h. N₂ physisorption experiments were carried out at –196 °C on a Quadrasorb apparatus (Quantachrome Instruments, USA). Specific surface areas (SSA) of the materials are calculated using the multipoint Brunauer–Emmett–Teller (BET) model in the relative pressure range of 0.05 – 0.2. The total pore volumes (V_t) were determined at $p/p_0 = 0.99$. The pore size distributions are calculated using quenched solid density functional theory (QSDFT) method for nitrogen on carbon with slit/cylindrical/spherical pores at –196 °C, adsorption branch kernel, integrated into the QuadraWin™ 5.11 analysis software (Quantachrome). Water and chiral gas physisorption measurements were performed using (S)-(+)-2-Butanol or (R)-(–)-2-Butanol at 25 °C (sample weight ~ 50 mg) on a Quantachrome Autosorb IQ apparatus.

Transmission electron microscopy

TEM was carried out on a TEM (EM 912 Omega/Carl-Zeiss Oberkochen) operating at 120 kV. Before analysis, the samples were dispersed in ethanol, and several droplets were cast onto copper TEM grids with a holey carbon film and then dried at room temperature.

Scanning electron microscopy

SEM was carried out on a LEO 1550-Gemini microscope operating at 3.00 kV. The samples were coated with a few nm thin platinum layer via sputtering to increase the surface conductivity.

Powder x-ray diffraction

PXRD patterns were recorded on a Bruker D8 Advance diffractometer equipped with a scintillation counter detector with CuK α radiation ($\lambda = 0.1518$ nm) applying 2θ step size of 0.02 ° and counting time of 1 s per step.

Thermogravimetric analysis

TGA measurements were performed using a Thermo Microbalance TG 209 F1 Libra (Netzsch, Selb, Germany). A platinum crucible was used for the measurements of 10 ± 1 mg of samples in nitrogen flow of 20 mL min^{-1} and oxygen purge flow of 10 mL min^{-1} . The sample was heated to $1000 \text{ }^\circ\text{C}$ with a heating rate of $10 \text{ }^\circ\text{C min}^{-1}$. The data was recorded and analyzed by the Proteus (6.0.0) software package.

Thermogravimetric analysis coupled with mass spectrometry

TGA-MS measurements were performed using a Thermo Microbalance TG 209 F1 Libra (Netzsch, Selb, Germany) coupled with a Thermostar Mass spectrometer (Pfeiffer Vacuum; Asslar/Germany) with ionization energy of 75eV. A platinum crucible was used for the measurement of 10 ± 1 mg of samples in a helium flow of 10 mL min^{-1} and a purge flow of 10 mL min^{-1} . The samples have been heated to $910 \text{ }^\circ\text{C}$ with a heating rate of $2.5 \text{ }^\circ\text{C min}^{-1}$. Data have been recorded and analyzed by the Proteus (6.1.0) and Quadstar (7.03, MID modus) software package.

Elemental analysis

C/H/N/S elemental analysis (EA) was accomplished as a combustion analysis using a Vario Micro device.

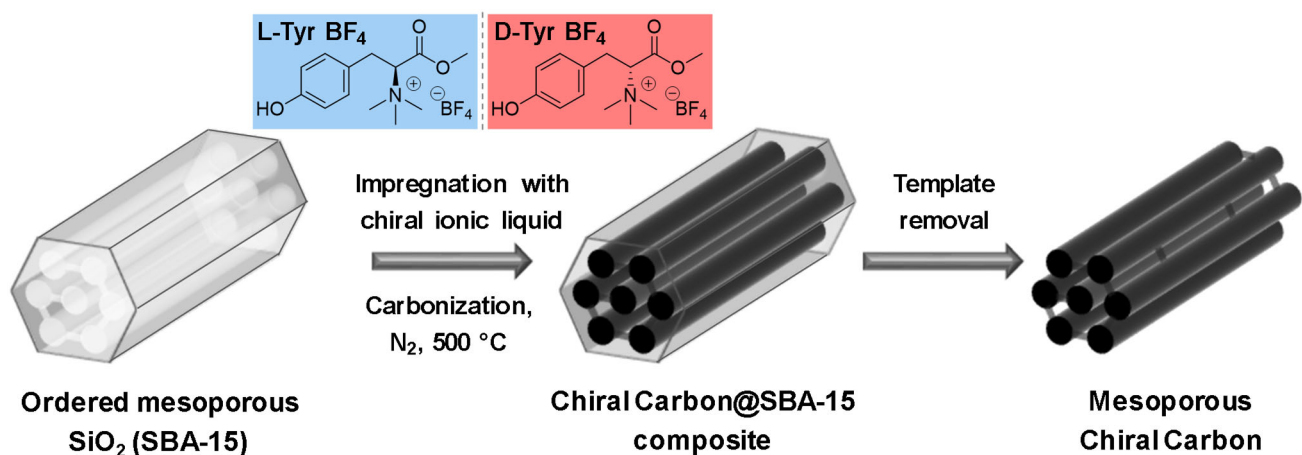
Isothermal titration calorimetry

ITC measurements were performed using a VP-ITC microcalorimeter from MicroCal (Northampton, USA). Two identical spherical cells, a reference cell, and a sample cell, both with a volume of 1.442 mL, were enclosed in an adiabatic jacket. The working cell was filled with an aqueous dispersion of the sample, and the reference cell was filled with water. The titrant (20 mM L-Phenylalanine or 20 mM D-Phenylalanine) was injected stepwise into the working cell with a syringe of the total volume of 288 μL . The sample cell was constantly stirred at a stirring rate of 307 rpm. The measurements were performed at a constant temperature of $25 \text{ }^\circ\text{C}$. Small aliquots of titrant (5 μL) were injected into the solution of the working cell. The first injection was set to a volume of 2 μL , because of the possible dilution during the

equilibration time preceding the measurement, and therefore the first injection was ignored in the analysis of the data. Spacing between the injections was set to 300 s. Data analysis was performed using the Origin software provided by MicroCal. The enantiomeric ratio of carbons for Phenylalanine is calculated as the ratio of integrated ITC peaks.

3. Results and Discussion

Two mesoporous carbon materials each with different chiral information were synthesized by infiltration of the ordered mesoporous silica template, SBA-15, with a solution of one enantiomer of a chiral ionic liquid and trimesic acid, followed by carbonization and subsequent template removal (**Scheme 1**). Chiral ionic liquids, N,N,N-trimethyl-L-Tyrosine methyl ester tetrafluoroborate, and its D-enantiomer, were synthesized by a previously reported procedure.^{40, 43} CIL and trimesic acid were used as chiral carbon precursor, and a crosslinking agent, respectively. Chiral carbons are labeled as L-m-carbon and D-m-carbon, where “m” stands for “mesoporous”. A comparably low carbonization temperature of 500°C has been chosen to minimize decomposition and unwanted reactions of the functional groups carrying the chiral information.



Scheme 1. Graphical presentation of the synthesis procedure of mesoporous chiral carbons.

Nitrogen physisorption experiments ($-196\text{ }^{\circ}\text{C}$) reveal that the two carbon materials prepared from different enantiomers of CIL have a comparable porosity with a predominantly mesoporous structure (**Figure 1a, b**, and **Table 1**). They display a type II isotherm with an H3 hysteresis loop, indicating a gradual monolayer – multilayer coverage and a non-rigid nature of these materials. The latter is most likely as a consequence of the low temperature chosen for carbonization. No sign for major pore blocking or cavitation effects can be seen in the isotherms of both samples, which is an indication that the entire pore system is well accessible under the conditions of the measurement. There seems to be no significant contribution from bottle-neck-shaped pores. The pore size distribution (PSD) of L-m-carbon and D-m-carbon was analyzed using the quenched-solid density functional theory (QSDFT, adsorption branch kernel) for N_2 adsorbed on carbon with slit/cylindrical/spherical pore shape (**Figure 1b**).

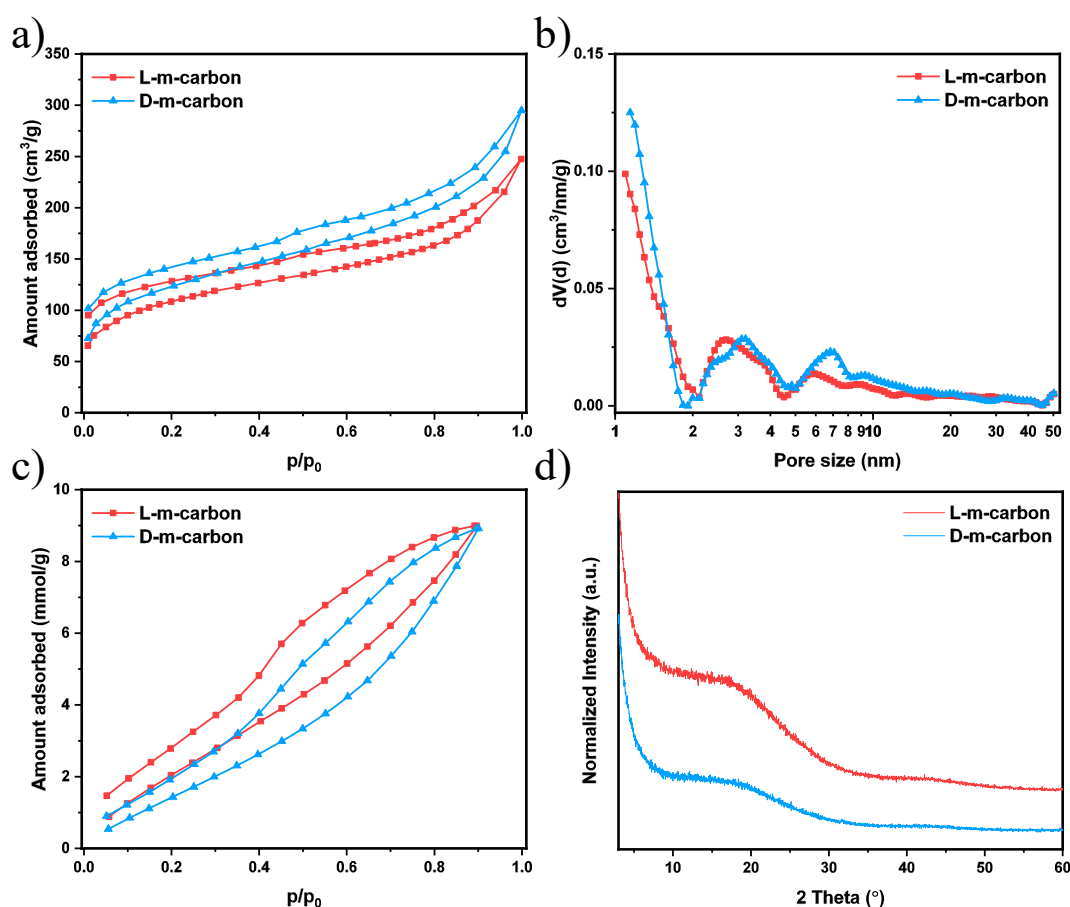


Figure 1. a) N₂ physisorption isotherms (at –196 °C) with the corresponding b) semi-logarithmic plots of differential pore size distribution calculated with QSDFT (N₂ on carbons with slit/cylindrical/spherical pores at 77 K, adsorption branch kernel), c) water vapor adsorption isotherms (at 25 °C), and d) PXRD patterns of L-m-carbon and D-m-carbon.

Table 1. Specific surface area (SSA_{BET}) calculated using the BET equation, DFT mesopore volume (V_{meso}), total pore volume (V_t).

Sample	SSA_{BET} (m ² /g)	V_{Meso} (cm ³ /g)	V_t (cm ³ /g)
L-m-carbon	391.1	0.24	0.38
D-m-carbon	441.1	0.29	0.46

Together with a small amount of micropores, the materials have a relatively broad size distribution of the larger mesopores, and narrow size distribution of smaller mesopores centered around 3 nm. L-m-carbon and D-m-carbon have comparable mesopore volumes of 0.24 and 0.29 cm³ g⁻¹, respectively (**Table 1**). The materials provide relatively high (multi-point) Brunauer–Emmett–Teller specific surface areas (SSA_{BET}) of 391.1 and 441.1 m² g⁻¹ for L- and D-enantiomer, respectively. Water adsorption isotherms (25 °C) show that the onset point of water adsorption is at comparably low relative pressures (**Figure 1c**). This reveals that the chiral carbons have relatively polar surface chemistry, due to the presence of heteroatoms and polar functional groups on the surface of the carbonaceous network. Water adsorption takes place over the entire pressure range of relative pressure as it is typical for materials with a broad pore size distribution. X-ray powder diffraction measurements (**Figure 1d**) of the samples indicate an x-ray amorphous structure without long-range order that is common for the high surface area carbons, and the absence of inorganic impurities.

Independent of the chirality of the applied CIL precursor, transmission electron microscopy (TEM) images show that some degree of directionality is present in the materials, which originates from the cylindrically shaped mesoporous hard template used in the synthesis (**Figure 2a**). The morphology appears rather open, revealing the large number of mesopores (**Figure 2**). Scanning electron microscopy (SEM) shows that L-m-carbon (**Figure 3a and b**) and D-m-carbon (**Figure 3c and d**) have a particle

morphology that is comparable to the SBA-15 template and is typical for hexagonally ordered mesoporous materials,⁴¹ which is in agreement with the observations from TEM measurements. These electron microscopy investigations are clearly revealing that the nanocasting approach can be successfully combined with the CILs as precursors and is thus applicable for the synthesis of porous carbon materials containing chiral information.

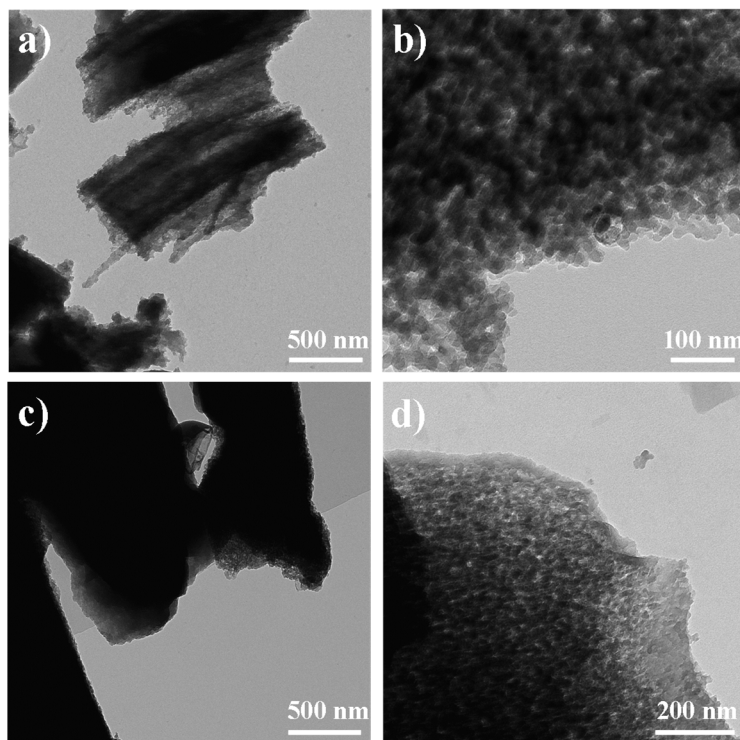


Figure 2. TEM images of a), b) L-m-carbon, and c), d) D-m-carbon.

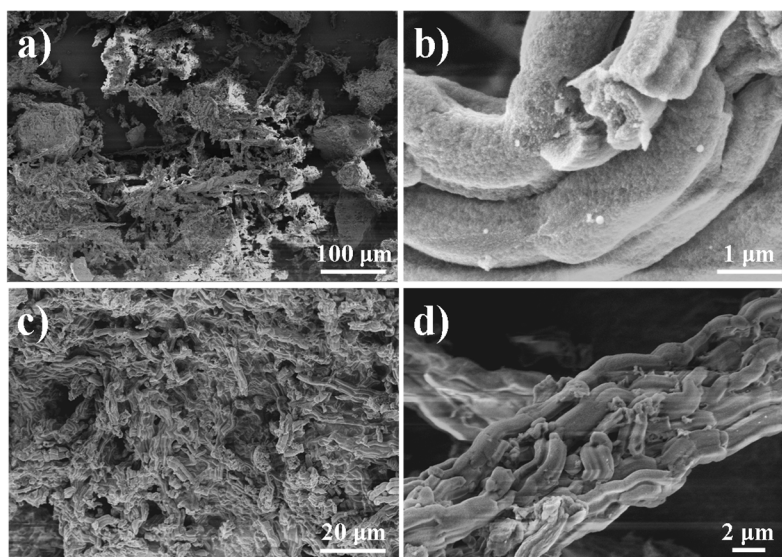


Figure 3. SEM images of a), b) L-m-carbon, and c), d) D-m-carbon.

Table 2. Elemental analysis and energy dispersive X-ray spectroscopy data summary of L-m-carbon and D-m-carbon. All the values are expressed in wt.%.

Sample	C		N		O _{EDX}	H _{EA}	S _{EA}	F _{EDX}
	EDX	EA	EDX	EA				
L-m-carbon	87.9	75.3	4.1	1.3	7.0	3.9	0.1	1.0
D-m-carbon	89.1	78.7	3.2	1.8	7.4	4.1	0.1	0.2

Thermogravimetric analysis (TGA) of the mesoporous materials was carried out under a flow of synthetic air (**Figure S1a**, Supporting Information). Both samples show small ash-content (less than 5 wt.%) at the temperatures above 500 °C, confirming the nearly complete removal of SBA-15 after carbonization and washing with NaOH. To investigate which chemical functionalities are present in the materials after the carbonization, TGA coupled with mass spectrometry (TGA-MS) under helium flow was employed (**Figure S1b**, **S2**, and **Figure S3**, Supporting Information). Mass loss of around 30 % until 900 °C under helium (**Figure S1b**, Supporting Information) points out that probably a high fraction of heteroatom-containing groups, together with some ordinary carbonization products are removed from the materials

since pure carbon materials are stable at high temperatures under an inert atmosphere. This observation is important because nitrogen is a constituent of the functional group carrying the chiral information in the chiral ionic liquid used as a precursor for the synthesis of mesoporous carbons (**Scheme 1**). Additionally, both materials demonstrate almost identical temperature profiles under synthetic air flow (**Figure S1a**, Supporting Information), as well as under helium flow (**Figure S1b**, Supporting Information). This suggests that they have a comparable chemical composition. Some of the most notable TGA-MS peaks emerging both for L-m-carbon (**Figure S2**, Supporting Information) and D-m-carbon (**Figure S3**, Supporting Information) are m/z 30, which is often denoted as a nitrogen indicator, 15 belonging to either NH or CH₃. m/z 26 is caused by CN or C₂H₂, and m/z 78 originates from the benzene ring in the form of C₆H₆. The results of C/H/N/S elemental analysis (EA) and energy dispersive X-ray spectroscopy (EDX) confirm the comparable content of nitrogen in both samples (**Table 2**). The remaining content of non-detected contributions of elemental analysis of both carbons is also comparable, 19 wt.% in L-m-carbon, and 15 wt.% in D-m-carbon. This can be partially attributed to covalently bonded oxygen-containing groups, as the O content determined by EDX is 7.0 and 7.4 wt.%, for L- and D-m-carbon, respectively. In addition, the heteroatom doping in these materials causes a comparably polar surface, and thus the adsorption of moisture and other oxygen-containing gases from the atmosphere can be another reason for the non-detected contributions in EA. Since the ash-content above 500 °C determined by TGA is less than 5 wt.%, there seems to be no major content of inorganic impurities. Structural characterization of L-m-carbon and D-m-carbon demonstrates that they have very similar porosity, morphology, and chemical composition of the bulk, as well as the surface of the materials. Therefore, it is expected that the differences in their interactions with enantiopure species from the solution, or the gas phase, will be caused by the chiral surface of these carbon materials.

To determine the chiral nature of the synthesized materials, isothermal titration calorimetry (ITC) was employed (**Figure 4**).^{39-40, 44} This technique is used to determine the thermodynamic parameters of

interactions in solution, and can, therefore, be used for measuring the released or absorbed heat upon mixing of enantiopure compounds with chiral materials. L-Phenylalanine (upper panel), and D-Phenylalanine (lower panel) were injected into dispersions of L-m-carbon (**Figure 4a**) and D-m-carbon (**Figure 4b**). From the results of ITC, it can be concluded that specific interactions between the enantiomers of amino acid and carbon dispersed in water are occurring. Upon injection, the amino acid molecules adsorb on the pore walls of the chiral carbon, which has to be preceded by desorption of water from the pore and its release in the bulk solution. The differences between the heat flow during adsorption of the chiral compound and the heat flow caused by water desorption are then recorded as an ITC signal. L-m-carbon has a stronger interaction with D-Phenylalanine, with maximum heat flow of $25 \mu\text{J sec}^{-1}$ per injection than with L-Phenylalanine, with maximum heat flow of $15 \mu\text{J sec}^{-1}$ per injection (**Figure 4a**). As expected, the opposite trend is observed for D-m-carbon, which has a stronger interaction with L-Phenylalanine (maximum heat flow $17 \mu\text{J sec}^{-1}$ per injection), than with D-Phenylalanine (maximum heat flow $12 \mu\text{J sec}^{-1}$ per injection) (**Figure 4b**).

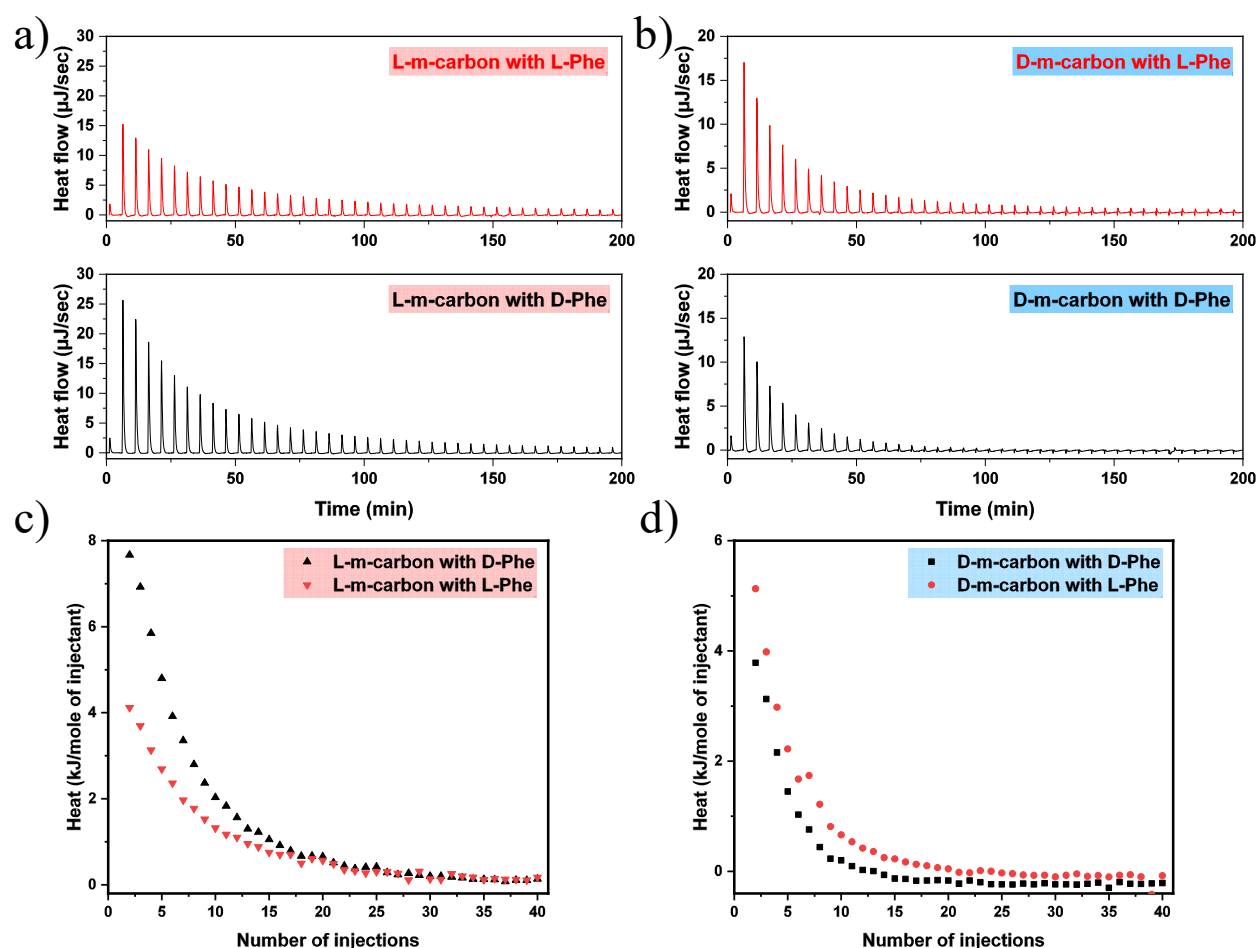


Figure 4. a) and b) Raw isothermal titration calorimetry data from injecting L-Phenylalanine (upper panel), and D-Phenylalanine (lower panel), into dispersions of a) L-m-carbon, and b) D-m-carbon. Heat per mole of injected D-Phenylalanine (black points), and L-Phenylalanine (red points), into a dispersion of c) L-m-carbon, and b) D-m-carbon.

Integrating the individual heat flow peaks gives a more precise and quantitative overview over the heat of each injection (**Figure 4c–d**), and highlights the chiral nature of the materials even more obviously than raw ITC data. Interaction between L-m-carbon and D-Phenylalanine causes the heat of 7.7 kJ mol^{-1} per injection, in comparison to interaction with L-Phenylalanine with a maximum of 4.1 kJ mol^{-1} per injection (**Figure 4c**). On the other hand, injecting L-Phenylalanine into D-m-carbon dispersion reaches 5.1 kJ mol^{-1} , and injecting D-Phenylalanine yields in less than 3.8 kJ mol^{-1} per injection (**Figure 4d**). The differences between the chiral carbon adsorbents are more pronounced over the first injections because it can be assumed that the Phenylalanine molecules interact with the sites providing the strongest

adsorption (and by that the most selective chiral recognition) at the lowest concentration. From this we can express the enantiomeric ratio of L-m-carbon for Phenylalanine to be $(D/L) = 1.88$, and of D-m-carbon $(L/D) = 1.34$.

The control experiments with ITC were conducted by titrating the amino acid solutions into pure water, a dispersion of commercial activated carbon (AC) material, or a solution of precursor CIL (**Figure S4 and S5**, Supporting Information). From this it is possible to conclude approximate heat of dilution (injection of Phenylalanine into water), which equals to 0.8 kJ mol^{-1} per injection. Injection of Phenylalanine into dispersion of AC, or when no specific interactions are taking place, causes 4.7 kJ mol^{-1} per injection (**Figure S4**, Supporting Information). Also when amino acid is titrated into solution of chiral ionic liquid (L-Tyr BF_4 and D-Tyr BF_4), no specific interactions were observed, with released heat in the range of heat of dilution (**Figure S5**, Supporting Information).

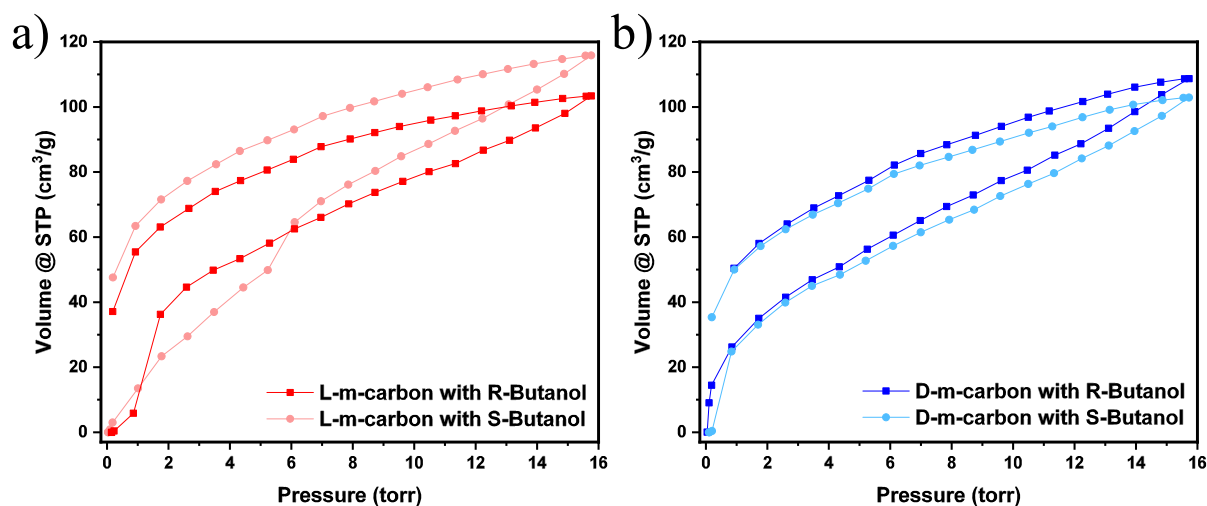


Figure 5. Chiral (R)-(-)-2-Butanol and (S)-(+)-2-Butanol vapor adsorption isotherms (at $25 \text{ }^\circ\text{C}$) a) L-m-carbon, and b) D-m-carbon.

Another technique employed to investigate the chiral recognition of the materials is the physisorption of chiral vapor. In comparison to ITC measurements, this method has the advantage that there are only two phases involved in the adsorption process and interfering solvent effects can be ruled out. For these

experiments, (R)-(-)-2-Butanol and (S)-(+)-2-Butanol were adsorbed on both enantiomers of carbon materials. Adsorption isotherms of chiral vapors on L-m-carbon reveal a higher affinity of this material towards S-Butanol than towards R-Butanol (**Figure 5a**). D-m-carbon shows the opposite behavior, with higher total uptake of R-Butanol than S-Butanol (**Figure 5b**), which underlines the results of ITC and shows that the chiral recognition of the materials is not limited to the enantioselective adsorption of species from solutions.

Conclusion

Chiral carbon containing meso- and micropores have been synthesized by the nanocasting technique from chiral ionic liquid precursors, and have been exemplarily applied for chiral separation in gas and liquid phase. To decrease the amount of non-discriminative surface and to maximize the accessibility of the surface, mesopores have been introduced in the materials by the means of nanocasting with silica template. In this way, larger compounds can be efficiently separated as well, and adsorption equilibria can be reached faster. Another possible advantage is that the enantioselective adsorption of compounds in mesopores may not be overshadowed by strong adsorption enthalpy arising from adsorption in the micropores and thus higher selectivity can be achieved. It was shown that mesoporous L-m-carbon and D-m-carbon interact strongly with the chiral species from the liquid phase, and exhibit preferred interaction with one enantiomer of the same compound. Similarly, adsorption from the gas phase is higher for one enantiomer of chiral vapor than for the other. These findings have to be transferred to adsorption and conversion of compounds from racemic mixtures but are a significant step towards the application of thermally and chemically stable carbon materials which can enable new applications in fields such as chiral separation, and possibly in asymmetric catalysis. Clearly, the chiral recognition of these functionalized carbon materials is still far behind the one achievable with established compounds such as silica or MOFs but the present study reports a first attempt to utilize the nanocasting concept to achieve control over the porosity in the resulting chiral carbons. It can be expected that the transfer of

this approach towards precursor molecules with a higher density of chiral sites will make it possible to efficiently utilize the advantages of porous carbon materials such as high chemical stability, electrical conductivity, and tailorable pore size in applications ranging from chiral separation to chiral (electro)catalysis.

Acknowledgments

The authors kindly acknowledge contributions from our colleagues at the Max Planck Institute of Colloids and Interfaces. Many thanks to Rona Pitschke and Heike Runge (TEM and SEM), Antje Völkel (TGA and elemental analysis), and Jessica Brandt for the help with ITC measurements. This research was supported by the German-Israeli Foundation for Scientific Research and Development (GIF, Grant No. I-87-302.10-2015).

Associated Content

Supporting information. Thermal analysis of L-m-carbon and D-m-carbon under synthetic air, and helium; MS ion currents obtained from TGA-MS measurement of L-m-carbon and D-m-carbon under helium; Integrated ITC data.

References

1. Ma, W.; Xu, L.; de Moura, A. F.; Wu, X.; Kuang, H.; Xu, C.; Kotov, N. A., Chiral Inorganic Nanostructures. *Chem. Rev.* **2017**, *117* (12), 8041-8093.
2. Scriba, G. K. E., Chiral recognition in separation science – an update. *J. Chromatogr. A* **2016**, *1467*, 56-78.
3. Basheer, A. A., Chemical chiral pollution: Impact on the society and science and need of the regulations in the 21st century. *Chirality* **2018**, *30* (4), 402-406.
4. Lesellier, E.; West, C., The many faces of packed column supercritical fluid chromatography – A critical review. *J. Chromatogr. A* **2015**, *1382*, 2-46.
5. Xie, S.-M.; Yuan, L.-M., Recent progress of chiral stationary phases for separation of enantiomers in gas chromatography. *J. Sep. Sci.* **2017**, *40* (1), 124-137.
6. Mehnert, C. P.; Cook, R. A.; Dispenziere, N. C.; Afeworki, M., Supported Ionic Liquid Catalysis – A New Concept for Homogeneous Hydroformylation Catalysis. *J. Am. Chem. Soc.* **2002**, *124* (44), 12932-12933.
7. Che, S.; Liu, Z.; Ohsuna, T.; Sakamoto, K.; Terasaki, O.; Tatsumi, T., Synthesis and characterization of chiral mesoporous silica. *Nature* **2004**, *429* (6989), 281-284.

8. Shopsowitz, K. E.; Kelly, J. A.; Hamad, W. Y.; MacLachlan, M. J., Biopolymer Templated Glass with a Twist: Controlling the Chirality, Porosity, and Photonic Properties of Silica with Cellulose Nanocrystals. *Adv. Funct. Mater.* **2014**, *24* (3), 327-338.
9. Shopsowitz, K. E.; Qi, H.; Hamad, W. Y.; MacLachlan, M. J., Free-standing mesoporous silica films with tunable chiral nematic structures. *Nature* **2010**, *468* (7322), 422-425.
10. Van de Voorde, B.; Bueken, B.; Denayer, J.; De Vos, D., Adsorptive separation on metal-organic frameworks in the liquid phase. *Chem. Soc. Rev.* **2014**, *43* (16), 5766-5788.
11. Cui, Y.; Li, B.; He, H.; Zhou, W.; Chen, B.; Qian, G., Metal-Organic Frameworks as Platforms for Functional Materials. *Acc. Chem. Res.* **2016**, *49* (3), 483-493.
12. Ma, L. Q.; Abney, C.; Lin, W. B., Enantioselective catalysis with homochiral metal-organic frameworks. *Chem. Soc. Rev.* **2009**, *38* (5), 1248-1256.
13. Padmanaban, M.; Müller, P.; Lieder, C.; Gedrich, K.; Grünker, R.; Bon, V.; Senkovska, I.; Baumgärtner, S.; Opelt, S.; Paasch, S.; Brunner, E.; Glorius, F.; Klemm, E.; Kaskel, S., Application of a chiral metal-organic framework in enantioselective separation. *Chem. Commun.* **2011**, *47* (44), 12089-12091.
14. Han, Z.; Wang, K.; Guo, Y.; Chen, W.; Zhang, J.; Zhang, X.; Siligardi, G.; Yang, S.; Zhou, Z.; Sun, P.; Shi, W.; Cheng, P., Cation-induced chirality in a bifunctional metal-organic framework for quantitative enantioselective recognition. *Nat. Commun.* **2019**, *10* (1), 5117.
15. Qin, Q.; Heil, T.; Antonietti, M.; Oschatz, M., Single-Site Gold Catalysts on Hierarchical N-Doped Porous Noble Carbon for Enhanced Electrochemical Reduction of Nitrogen. *Small Methods* **2018**, *2* (12), 1800202.
16. Simon, P.; Gogotsi, Y., Materials for electrochemical capacitors. *Nature Materials* **2008**, *7* (11), 845-854.
17. Tiwari, J. N.; Vij, V.; Kemp, K. C.; Kim, K. S., Engineered Carbon-Nanomaterial-Based Electrochemical Sensors for Biomolecules. *ACS Nano* **2016**, *10* (1), 46-80.
18. Francke, R.; Little, R. D., Optimizing Electron Transfer Mediators Based on Arylimidazoles by Ring Fusion: Synthesis, Electrochemistry, and Computational Analysis of 2-Aryl-1-methylphenanthro[9,10-d]imidazoles. *J. Am. Chem. Soc.* **2014**, *136* (1), 427-435.
19. Guo, P.; Wong, K.-Y., Enantioselective electrocatalytic epoxidation of olefins by chiral manganese Schiff-base complexes. *Electrochem. Commun.* **1999**, *1* (11), 559-563.
20. Nishitani, S.; Sekiya, R.; Haino, T., Chirality-Embedded Nanographenes. *Angew. Chem. Int. Ed.* **2020**, *59* (2), 669-673.
21. Suzuki, N.; Wang, Y.; Elvati, P.; Qu, Z.-B.; Kim, K.; Jiang, S.; Baumeister, E.; Lee, J.; Yeom, B.; Bahng, J. H.; Lee, J.; Violi, A.; Kotov, N. A., Chiral Graphene Quantum Dots. *ACS Nano* **2016**, *10* (2), 1744-1755.
22. Filippone, S.; Maroto, E. E.; Martín-Domenech, Á.; Suarez, M.; Martín, N., An efficient approach to chiral fullerene derivatives by catalytic enantioselective 1,3-dipolar cycloadditions. *Nat. Chem.* **2009**, *1* (7), 578-582.
23. Karousis, N.; Tagmatarchis, N.; Tasis, D., Current Progress on the Chemical Modification of Carbon Nanotubes. *Chem. Rev.* **2010**, *110* (9), 5366-5397.
24. Oschatz, M.; Walczak, R., Crucial Factors for the Application of Functional Nanoporous Carbon-Based Materials in Energy and Environmental Applications. *C* **2018**, *4* (4), 56.
25. Paraknowitsch, J. P.; Thomas, A., Functional Carbon Materials From Ionic Liquid Precursors. *Macromol. Chem. Phys.* **2012**, *213* (10-11), 1132-1145.
26. Liu, J.; Wickramaratne, N. P.; Qiao, S. Z.; Jaroniec, M., Molecular-based design and emerging applications of nanoporous carbon spheres. *Nature Materials* **2015**, *14* (8), 763-774.
27. Lu, A.-H.; Zhao, D.; Wan, Y., *Nanocasting: A Versatile Strategy for Creating Nanostructured Porous Materials*. The Royal Society of Chemistry: Cambridge, **2009**.
28. White, R. J.; Tauer, K.; Antonietti, M.; Titirici, M.-M., Functional Hollow Carbon Nanospheres by Latex Templating. *J. Am. Chem. Soc.* **2010**, *132* (49), 17360-17363.
29. Perovic, M.; Qin, Q.; Oschatz, M., From Molecular Precursors to Nanoparticles—Tailoring the Adsorption Properties of Porous Carbon Materials by Controlled Chemical Functionalization. *Adv. Funct. Mater.* **2020**, doi: 10.1002/adfm.201908371, 1908371.

30. Borchardt, L.; Zhu, Q.-L.; Casco, M. E.; Berger, R.; Zhuang, X.; Kaskel, S.; Feng, X.; Xu, Q., Toward a molecular design of porous carbon materials. *Mater. Today* **2017**, *20* (10), 592-610.
31. Stein, A.; Wang, Z.; Fierke, M. A., Functionalization of Porous Carbon Materials with Designed Pore Architecture. *Adv. Mater.* **2009**, *21* (3), 265-293.
32. Walczak, R.; Savateev, A.; Heske, J.; Tarakina, N. V.; Sahoo, S.; Epping, J. D.; Kühne, T. D.; Kurpil, B.; Antonietti, M.; Oschatz, M., Controlling the strength of interaction between carbon dioxide and nitrogen-rich carbon materials by molecular design. *Sustainable Energy Fuels* **2019**, *3*, 2819.
33. Walczak, R.; Kurpil, B.; Savateev, A.; Heil, T.; Schmidt, J.; Qin, Q.; Antonietti, M.; Oschatz, M., Template- and Metal-Free Synthesis of Nitrogen-Rich Nanoporous “Noble” Carbon Materials by Direct Pyrolysis of a Preorganized Hexaazatriphenylene Precursor. *Angew. Chem. Int. Ed.* **2018**, *57* (33), 10765-10770.
34. Fechler, N.; Zussblatt, N. P.; Rothe, R.; Schlögl, R.; Willinger, M.-G.; Chmelka, B. F.; Antonietti, M., Eutectic Syntheses of Graphitic Carbon with High Pyrazinic Nitrogen Content. *Adv. Mater.* **2016**, *28* (6), 1287-1294.
35. Mahmood, J.; Lee, E. K.; Jung, M.; Shin, D.; Jeon, I.-Y.; Jung, S.-M.; Choi, H.-J.; Seo, J.-M.; Bae, S.-Y.; Sohn, S.-D.; Park, N.; Oh, J. H.; Shin, H.-J.; Baek, J.-B., Nitrogenated holey two-dimensional structures. *Nat. Commun.* **2015**, *6*, 6486.
36. Lee, J.; Kim, J.; Hyeon, T., Recent Progress in the Synthesis of Porous Carbon Materials. *Adv. Mater.* **2006**, *18* (16), 2073-2094.
37. Lu, A.-H.; Schüth, F., Nanocasting: A Versatile Strategy for Creating Nanostructured Porous Materials. *Adv. Mater.* **2006**, *18* (14), 1793-1805.
38. Xia, Y.; Yang, Z.; Mokaya, R., Templated nanoscale porous carbons. *Nanoscale* **2010**, *2* (5), 639-659.
39. Fuchs, I.; Fechler, N.; Antonietti, M.; Mastai, Y., Enantioselective Nanoporous Carbon Based on Chiral Ionic Liquids. *Angew. Chem. Int. Ed.* **2015**, *55* (1), 408-412.
40. Aloni, S. S.; Perovic, M.; Weitman, M.; Cohen, R.; Oschatz, M.; Mastai, Y., Amino acid-based ionic liquids as precursors for the synthesis of chiral nanoporous carbons. *Nanoscale Advances* **2019**, *1* (12), 4981-4988.
41. Yan, R.; Heil, T.; Presser, V.; Walczak, R.; Antonietti, M.; Oschatz, M., Ordered Mesoporous Carbons with High Micropore Content and Tunable Structure Prepared by Combined Hard and Salt Templating as Electrode Materials in Electric Double-Layer Capacitors. *Adv. Sustainable Syst.* **2017**, *2*, 1700128.
42. Zhao, D.; Feng, J.; Huo, Q.; Melosh, N.; Fredrickson, G. H.; Chmelka, B. F.; Stucky, G. D., Triblock Copolymer Syntheses of Mesoporous Silica with Periodic 50 to 300 Angstrom Pores. *Science* **1998**, *279* (5350), 548-552.
43. Silva, S. G.; Rodríguez-Borges, J. E.; Marques, E. F.; do Vale, M. L. C., Towards novel efficient monomeric surfactants based on serine, tyrosine and 4-hydroxyproline: synthesis and micellization properties. *Tetrahedron* **2009**, *65* (21), 4156-4164.
44. Shval, A.; Mastai, Y., Isothermal titration calorimetry as a new tool to investigate chiral interactions at crystal surfaces. *Chem. Commun.* **2011**, *47* (20), 5735-5737.